Analysis of Gas Chromatography Pulse Dispersion Data for the System *n*-Butane/Zeolite NaY

An analysis of gas chromatography pulse dispersion data for the system *n*-butane/zeolite NaY is presented. The data were analyzed in terms of two models, an intracrystalline diffusion limiting model and a surface barrier model. Both models provided acceptable fits to the pulse dispersion data; however, the temperature dependence of the apparent mass transport parameters strongly suggests that a surface barrier is responsible for the observed transport resistance. The Henry's law constants were independent of choice of model and the isosteric heat of sorption was consistent with literature values.

Chen-Chen Fu, M. S. P. Ramesh, H. W. Haynes, Jr.
Chemical Engineering Department
University of Wyoming
Laramie, WY 82071

SCOPE

There are indications in the literature that diffusion measurements in zeolites by the sorption rate technique may under certain circumstances be controlled by a surface barrier resistance. This is most likely to occur for rapid diffusion in small crystals of large-pore zeolites. However, another phenomenon must be considered in analyzing such systems, namely the sorption heat effect. Failure to take into account either the surface barrier or the sorption heat effect will result in erroneously low reported values of intracrystalline diffusivity. It is important to distinguish between these effects because of the many applications of large-pore zeolites in industry.

Pulse gas chromatography offers a potential means for eliminating the sorption heat effect, and at the same time it should be sensitive to a surface barrier. In the present study we have undertaken a study of *n*-butane sorption and diffusion on a commercial sample of zeolite NaY. The data are analyzed on the basis of an intracrystalline diffusion model and a surface barrier model. We earlier reported results on the *n*-butane/NaY system, but it was not possible to obtain quantitative results due to a system nonlinearity (Hsu and Haynes, 1981). This problem was eliminated in the present study by using much more sensitive detectors.

CONCLUSIONS AND SIGNIFICANCE

By injecting highly diluted *n*-butane pulses into our system it was possible to operate in a linear region where complications from nonlinear sorption, non-Fickian diffusion and sorption heat effects were absent. Henry's law constants were independent of the choice of model, and the isoteric heat of sorption compared favorably with literature values on a similar zeolite (NaX). It was not possible to distinguish between an intracrystalline diffusion model and a surface barrier model on the basis of goodness of fit. However, arguments based on the apparent activation energies support the surface barrier model. Furthermore, it appears that the surface barrier is due to a finite rate of adsorption from the gas phase, as opposed to pore constrictions just under the zeolite crystal surface. This interpretation leads to the conclusion that the sticking coefficient for molecules colliding with the external surface is of the order of 10^{-7}. Such a small value of the

Correspondence concerning this paper should be addressed to H. W. Haynes, Jr.

sticking coefficient is suggestive of an immobile or restricted transition state at the entrance to the zeolite crystal.

It is important to realize that our study employed very small crystals of a large-pore zeolite, and it is therefore not unreasonable that the surface barrier resistance should dominate. In other studies of diffusion in large crystals and/or small-pore zeolites, the intracrystalline diffusion resistance may well dominate. A general analysis must account for both effects, but it may not be possible to separate these effects on the basis of goodness of fit.

Introduction

The techniques that have been employed to evaluate intracrystalline diffusivities in zeolites include sorption rate, plus chromatography, and nuclear magnetic resonance (Ruthven, 1983; 1984). The first two approaches are ideally suited to measurements in slowly diffusing systems ($D < 10^{-7}$ cm^2/s), whereas the NMR method is applicable when diffusion is rapid ($5 \times 10^{-8} < D < 10^{-4}$ cm^2/s). As demonstrated by Shah and Ruthven (1977), results from the sorption rate and pulse chromatography methods compare favorably, at least for slowly diffusing systems. Despite there being little overlap for comparison of sorption rate and NMR diffusivities, some success has been achieved (Kärger and Ruthven, 1981). Typically, however, one obtains apparent intracrystalline diffusivities by the sorption rate method that are several orders of magnitude smaller than NMR values. This is especially true for small crystals and/or large-pore zeolites.

A possible explanation for this discrepancy becomes apparent when sorption rates are determined as a function of crystallite size. Contrary to theory, several investigators have observed an effect of crystallite size on the apparent diffusivity (Kärger and Caro, 1977; Bülow et al., 1980). The most striking example is provided by Kärger and Caro, who compared methane diffusivities in chabazites obtained by the sorption rate and NMR techniques for a wide range of crystallite sizes. The NMR values were invariant at about 10^{-6} cm^2/s. In sharp contrast, the sorption rate values increased monotonically with crystallite size from about 10^{-10} cm^2/s in five-micron particles to ultimately approach the NRM values in crystals larger than two thousand microns. In these experiments the sorption rate measurements in small crystallites were clearly not limited by intracrystalline diffusion, and it was proposed that the measurements might instead be reflecting a resistance at the external surface of the crystal, i.e., a surface barrier. As the crystallite size becomes larger the intracrystalline diffusion resistance becomes significant due to the increased diffusion path, until ultimately intracrystalline diffusion dominates. A similar particle size effect was observed for *n*-paraffins diffusing in alkaline earth A-zeolites. The surface barrier model has also been applied to the sorption of gases on molecular sieve carbons (Koresh and Soffer, 1981).

The isothermicity assumption becomes questionable in rapidly diffusing systems due to the sorption heat effect, and herein lies an alternative explanation for the discrepancy between sorption rate and NMR diffusivities (Doelle and Riekert, 1979; Kärger and Ruthven, 1981; Bulow et al., 1984). Theoretical analyses indicate that the major resistance to heat transfer is at the external surface of the sample bed composed of individual crystals (Lee and Ruthven, 1979; Ruthven et al., 1980; Ruthven and Lee, 1981). Common practice is to test for the heat effect by varing the sample configuration (shallow bed vs. deep bed). If the isothermal model is curve-fit to an uptake curve for a nonisothermal system, one obtains erroneously small values of the diffusivity.

Both of these arguments cast doubt on the validity of reported sorption rate diffusivities for large-pore zeolites and/or small crystals. However, one should not discount the sorption rate measurements without first addressing the question of which factor is responsible for the erroneous diffusivity. If the heat effect is responsible, then the measurement is of little value (unless an appropriate correction can be applied). On the other hand, if a surface barrier is responsible, then might not the surface barrier also be important in a practical application of the zeolite?

Potentially, the pulse chromatography experiment offers a method of distinguishing between the surface barrier and thermal effects. The heat transfer characteristics of a packed chromatographic column are generally claimed to be superior to those of a low-pressure closed system such as that employed in the sorption rate determination. This is not to say that heat effects are never present in the pulse chromatography experiment, since Cerro and Smith (1969) demonstrated such an effect years ago. However, an analysis of thermal effects in the pulse chromatography experiment has shown that the demonstration of system linearity (by varying input pulse concentration) is sufficient to insure that no heat effect is present provided that the column is operating at infinite dilution. Details of this analysis will appear shortly (Haynes, 1986).

Several years ago we reported a study of the diffusion of hydrocarbons in zeolite NaY by the pulse chromatography technique (Hsu and Haynes, 1981). Normal butane was studied most extensively. It was not possible to report quantitative results in this study because of a nonlinear system response. Efforts to eliminate the nonlinearity by reducing pulse size ultimately resulted in loss of detector sensitivity. However, it seemed clear that a zeolite crystal-associated mass transfer resistance was in fact being observed. We have now repeated these experiments with *n*-butane using much more sensitive flame ionization detectors as opposed to the thermal conductivity detectors employed in the earlier study. With our new apparatus we are able to operate in the linear region where complicaitons from a nonlinear isotherm, non-Fickian, diffusion, and thermal effects are absent.

Theory

The mathematical model in its most general form is identical to that already described by Hsu and Haynes (1981). So is the method of analysis the same. (However, the earlier communication contains two typographical errors: the K_c in the numerator of Eq. 19 should be omitted, and a minus sign is needed in front of the integral of Eq. 26.) Consistent with the zeolite literature,

the model assumes that a single sorbed phase is present in the zeolite interior. In its most general form, the model includes the following mass transport mechanisms: axial dispersion, $\mathcal{D}_z$; external mass transport to the particle surface, k_f; intraparticle diffusion in the voids between compacted zeolite crystals, $\mathcal{D}_y$; finite rate of adsorption to the external surface of the zeolite crystal, k_a; and intracrystalline diffusion, $\mathcal{D}_c$. The model allows for a log-normal distribution of crystallite sizes.

Two simplifications of the model equations are considered in the present work. Under circumstances such that intracrystalline diffusion is the only significant particle-associated mass transport resistance, the model reduces to Eqs. 13, 18, 21, and 22 in Hsu and Haynes (1981). Working equations are obtained by transforming these equations into the frequency domain. Thus:

$$\tilde{E}(j\omega) = e^{D_1}\cos D_2 - je^{D_1}\sin D_2 \tag{1}$$

$$D_1 = \frac{vL}{2\mathcal{D}_z}\left(1 - \sqrt[4]{F_1^2 + F_2^2}\cos\theta/2\right) \tag{2}$$

$$D_2 = \frac{vL}{2\mathcal{D}_z}\sqrt[4]{F_1^2 + F_2^2}\sin\theta/2 \tag{3}$$

$$\theta = \tan^{-1}(F_2/F_1) \tag{4}$$

$$F_1 = 1 + 4\mathcal{D}_z G_1/v \tag{5}$$

$$F_2 = 4\mathcal{D}_z G_2/v \tag{6}$$

$$G_1 = \frac{1}{v}(1 - \theta_z)(1 - \theta_y)I_1 \tag{7}$$

$$G_2 = \frac{1}{v}\{[\theta_z + (1 - \theta_z)\theta_y]\omega + (1 - \theta_z)(1 - \theta_y)I_2\} \tag{8}$$

$$I_1 = \frac{3\mathcal{D}_c K_c}{\sqrt{\pi}\,R_x^3}\int_{-\infty}^{\infty} e^{-p^2} R_x(H_1 - 1)\,dp \tag{9}$$

$$I_2 = \frac{3\mathcal{D}_c K_c}{\sqrt{\pi}\,R_x^3}\int_{-\infty}^{\infty} e^{-p^2} R_x H_2\,dp \tag{10}$$

$$H_1 = \lambda\left(\frac{\sinh 2\lambda + \sin 2\lambda}{\cosh 2\lambda - \cos 2\lambda}\right) \tag{11}$$

$$H_2 = \lambda\left(\frac{\sinh 2\lambda - \sin 2\lambda}{\cosh 2\lambda - \cos 2\lambda}\right) \tag{12}$$

$$\lambda = R_x\sqrt{\omega/2\mathcal{D}_c} \tag{13}$$

$$R_x = \exp(\mu + \sqrt{2}\sigma p) \tag{14}$$

Equations 1 to 14 are working equations for the intracrystalline diffusion ($\mathcal{D}_c$) limiting case. Now suppose that intracrystalline diffusion is rapid and the rate of adsorption, k_a, at the external surface of the zeolite crystal controls the uptake rate. This is, in effect, the surface barrier model. Working equations for this case are identical to the above equations except for the functions I_1 and I_2, which must be replaced with:

$$I_1 = \frac{3k_a K_c^2\omega^2}{\sqrt{\pi}\,R_x^3}\int_{-\infty}^{\infty} e^{-p^2}\left(\frac{R_x^4}{9k_a^2 + R_x^2K_c^2\omega^2}\right)dp \tag{15}$$

$$I_2 = \frac{9k_a^2 K_c\omega}{\sqrt{\pi}\,R_x^3}\int_{-\infty}^{\infty} e^{-p^2}\left(\frac{R_x^3}{9k_a^2 + R_x^2K_c^2\omega^2}\right)dp \tag{16}$$

As pointed out in the earlier contribution, the integrals in these expressions for I_1 and I_2 are readily evaluated using the Gauss-Hermite quadrature formula.

There is one difference between our formulation of the surface barrier model and that of earlier workers (Kärger and Caro, 1977; Bülow et al., 1980). In the original investigations, the surface barrier was assumed to lie just under the zeolite surface. The resistance was presumed to arise from nonuniformities in zeolite structure at the crystal surface. Our picture is quite different in that a finite rate of adsorption from the gas phase is taken to be responsible for the surface barrier. According to our model the component flux entering the zeolite crystal is given by:

$$N = k_a(C_y - q/K_c) \tag{17}$$

where C_y is the gas phase concentration of diffusing component surrounding the zeolite crystal and q is the sorbed phase concentration at the crystal external surface. Earlier workers took the sorbed phase concentration as the driving force. The analogous equation is therefore:

$$N = k_s(C_y K_c - q) = k_s K_c(C_y - q/K_c) \tag{18}$$

The two interpretations of the surface barrier thus give identical working equations, and it is not possible to distinguish between the two by the pulse chromatography method. The coefficients are related according to:

$$k_a = k_s K_c \tag{19}$$

Experimental

The experimental apparatus is similar to the apparatus employed in the previous investigation (Hsu and Haynes, 1981), but with two major changes. As already mentioned, the thermal conductivity detectors of the original system were replaced with more sensitive flame ionization detectors (Gow Mac model 12-800). Another addition to the experimental set up is an automatic data acquisition system.

A simplified schematic of the apparatus is provided in Figure 1. Carrier gas from cylinder (1) is metered to the column through valve (8). The column pressure is set by a back-pressure regulator (12). A differential pressure cell (11) monitors pressure drop across the column (13). Flow rates are measured with rotameters (6). The diffusing component is introduced by means of a six-port sample injection valve (10). Generally the injection gas is a very dilute mixture of diffusing component in carrier. Samples are split from the inlet and outlet of the column and sent to the flame ionization detectors (15). Flow rates to the detectors are controlled by high-temperature metering valves (14). Signals from the detector electrometers are sent to a dual-

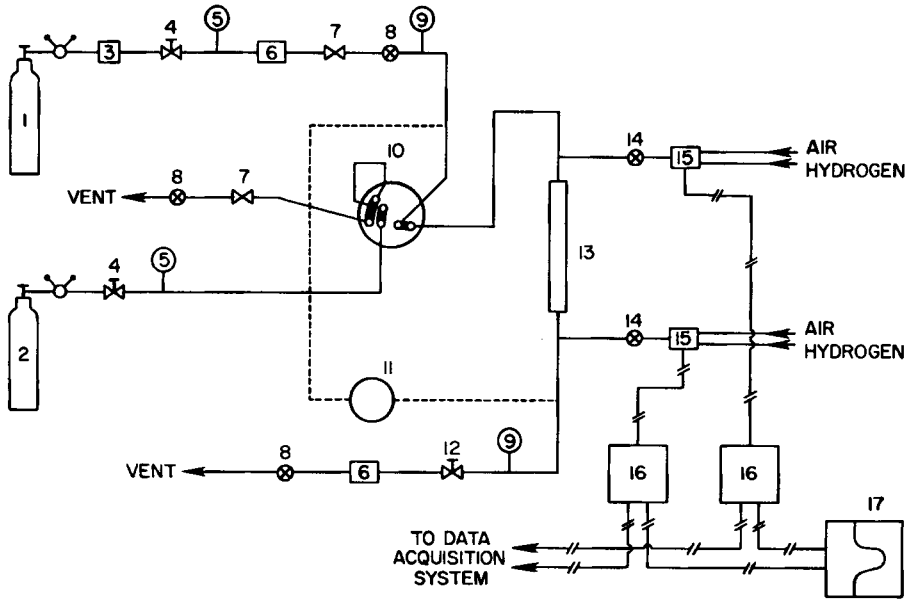

Figure 1. Pulse chromatography apparatus.

1. Carrier gas
2. Sample gas
3. Gas purifier
4. Pressure regulator
5. Pressure gauge
6. Rotameter
7. Cut-off valve
8. Metering valve
9. Pressure gauge
10. Sampling valve
11. Differential pressure gauge
12. Back presure regulator
13. Sample column
14. High-temperature metering valves
15. Flame ionization detectors
16. Electrometer
17. Dual pin recorder

pen strip chart recorder (17) for monitoring purposes only. The electrometer signals are amplified and sent to a Varex Universal Interface where both signals are digitized and stored in the interface memory. The Varex can sample at rates from 100 μs to 6 s between points with 8-bit resolution and can store up to 15,000 points per channel. Upon command from a Sage II microprocessor the data are transferred to a computer diskette. At the completion of the experiment the data are uploaded to our Cyber 730/760 main frame computer through the modem port on the Sage II.

Mixing in the valves (14) installed in the sample lines results in a tail in both the input and output curves. However, since the transfer functions of the two valves are identical, the effect cancels when the quotient of the output and input curves is taken in the frequency domain analysis. Although the self-correction for mixing in the valves is very good, a precise correction is not required due to the rapid time response of the valves relative to that of the column. More details are available in the thesis by Fu (1984).

The data workup is by the same procedure employed by Hsu and Haynes (1981). First the input and response curves are transformed to the frequency domain using Filon's integration method. The transformed residence time distribution curve (E curve) is computed by division in the frequency domain. The optimum parameter values are calculated from a comparison of the experimental frequency domain E curve with the theoretical E curve of Eq. 1. A Taylor series optimization procedure is used to obtain the optimum parameter values. The time domain E curves, both theoretical and experimental, are calculated by taking inverse Fourier transforms and the results are plotted using a computerized graphics package. The data manipulation is automatic until the optimum parameter values are computed and the time domain plot of theoretical and experimental E curves is produced.

The crystallite size distribution of the commercial zeolite (Linde LZ-Y52) was evaluated by several methods including video microscopy, conductometric, and sedimentation methods. Not unexpectedly there were significant differences between the various distributions even after correcting all to a common number fraction basis. The video microscopy distribution that was used in our earlier work was found to be skewed toward larger particles, as evidenced by agglomerates of up to 10 microns dia. visible under the SEM. The conductometric distributions differed from one another in a logical manner consistent with the orifice size chosen for the analysis. After careful consideration it was concluded that sedimentation of a predispersed sample of the zeolite would provide the most accurate crystallite size distribution for our sample. The experimental volume fraction distribution obtained by the sedimentation method is plotted in Figure 2, where log-normal behavior is indicated. Also plotted in this figure is the equivalent cumulative number fraction distribution that was actually employed in our calculations. The log-normal parameters are $\mu = -8.9604$ and $\sigma = 0.9036$ for the radius measured in cm. The average particle radius defined as $R_m = \overline{R_x^3}/\overline{R_x^2}$ is 8.80×10^{-5} cm.

The zeolite powder was pilled without a binder and crushed and sieved to two sizes, 20–30 and 30–40 mesh. Analysis by mercury porosimetry revealed a sharp macropore peak at about 2,000 Å radius. The macropore porosity was also calculated from the mercury porosimetry results. Two columns were prepared; specifications are given in Table 1. Prior to an experiment the column was heated to 250°C for 15 h under flowing helium.

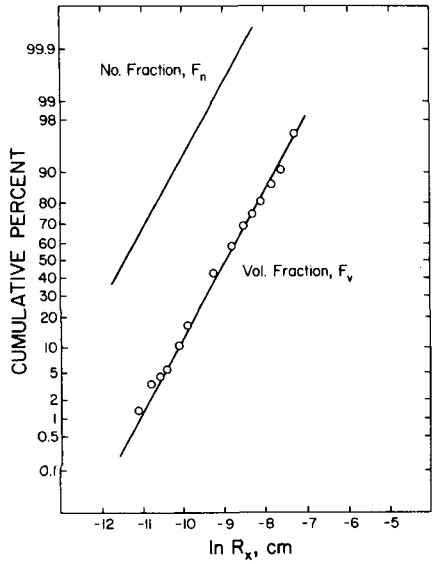

Figure 2. Crystallite size distribution.

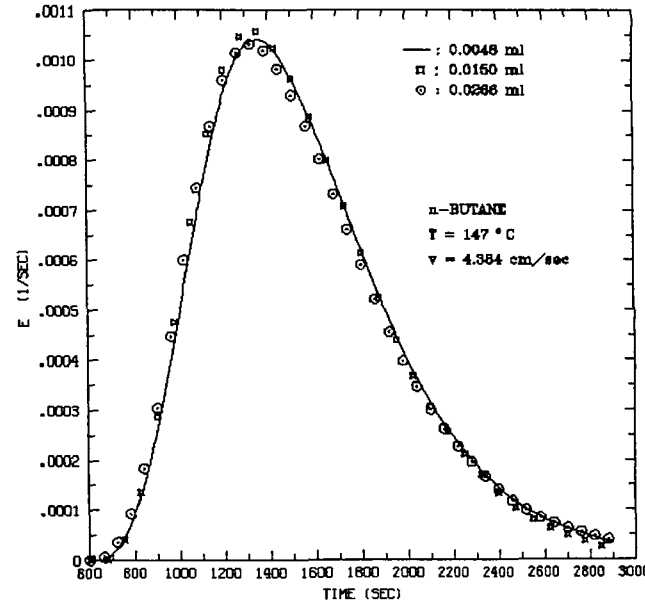

Figure 3. Effect of pulse size on experimental *E* curve.

All experiments were conducted at 16.3 psia (112.3 kPa) over temperatures ranging from 124 to 240°C. The carrier gas was high-purity helium.

Results

Since our earlier experiments were plagued by nonlinear system response, a series of experiments was conducted in order to test for linearity. Several dilute butane-helium mixtures were prepared and analyzed by gas chromatography. Pulses of these mixtures were then introduced into the column inlet and the corresponding E curves were compared in order to identify any concentration effect. The results of a typical linearity test are plotted in Figure 3. The E curves are essentially identical despite a greater than fivefold variation in the amount of butane injected. Thus in contrast to the previous study, the utilization of more sensitive detectors allows us to work well within the linear region.

Correlations for the axial dispersion coefficient were developed by the method of the previous study. Since small molecules such as methane diffuse very rapidly, the sole contributor to peak broadening is axial dispersion. The axial dispersion model was fitted to methane pulse data over a range of temperatures by a time domain regression (Hsiang and Haynes, 1977) and the values of $\mathcal{D}_z$ so obtained were correlated on a dimensionless plot of particle Peclet No. vs. Reynolds No. × Schmidt No. Ethane pulses over column 2 were treated identically and data for both components fell on the same curve. In our previous study argon and nitrogen dispersion coefficients when plotted in this manner coincided with results from the methane experiments. The fact that axial dispersion measurements from all these small molecules can be correlated on the same dimensionless plot supports the contention that particle-associated mass transport resistances are negligible in these experiments. Additional evidence is provided by the shape of the experimental E curve. In all cases the E curve was symmetrical, indicating that the axial dispersion contribution to peak broadening was dominant (Haynes, 1975; Chou, 1979). Axial dispersion data for column 1 were correlated with:

$$\frac{1}{Pe} = \frac{0.285}{Re\,Sc} + \frac{2.664}{1 + 0.239/Re\,Sc} \tag{20}$$

and for column 2 with:

$$\frac{1}{Pe} = \frac{0.363}{Re\,Sc} + 6.706\,Re\,Sc \tag{21}$$

Molecular diffusivities were calculated from the Chapman-Enskog kinetic theory.

Table 1. Column Details

	Column No. 1	Column No. 2
Length, cm	30.48	30.48
Inside dia., cm	1.09	1.09
Bed porosity	0.350	0.309
Particle mesh size	20/30	30/40
Avg. particle dia., mm	0.715	0.507
Macroporosity	0.486	0.497
Macropore radius, Å	2,000	2,000

Analysis based on intracrystalline diffusion model

The intracrystalline diffusion limiting model was fitted to the *n*-butane data with K_c and $\mathcal{D}_c$ as the adjustable parameters. The axial dispersion coefficient was calculated from the correlations of Eqs. 20 and 21. Computed results are summarized in Table 2. Typical time domain results illustrating goodness of fit are plotted in Figures 4 and 5. The data appear to be quite consistent with the model. Although the results are somewhat scattered, there is no consistent variation in diffusivity or Henry's law constant with particle size or velocity. In all respects the model appears to conform to model expectations.

Also plotted in Figures 4 and 5 is a curve fit of the model with $\mathcal{D}_c$ set equal to infinity. The only adjustable parameter in this

Table 2. Summary of Results

Run No.	Volume Injected μL	dp mm	T °C	v cm/s	$\mathcal{D}_z$ cm²/s	K_c^*	$\mathcal{D}_c \times 10^9$ cm²/s	K_c^{**}	$k_a \times 10^3$ cm/s
FURM 1-1	5.4	0.715	198	4.54	0.772	178.5	0.286	170.7	1.33
FURM 1-2	5.4	0.715	198	4.74	0.804	178.3	0.280	170.2	1.33
FURM 1-3	5.4	0.715	198	2.17	0.412	168.2	0.322	163.9	1.17
FURM 2-1	5.4	0.715	240	2.65	0.494	75.7	0.990	74.0	1.59
FURM 2-2	5.4	0.715	240	4.60	0.786	79.9	1.054	77.3	1.98
FURM 2-3	5.4	0.715	240	6.80	1.154	81.4	1.042	78.0	2.16
FURM 3-1	4.8	0.715	147	4.40	0.747	702	0.0406	657	0.87
FURM 3-2	26.6	0.715	147	4.40	0.747	698	0.0368	650	0.81
FURM 3-3	15.0	0.715	147	4.40	0.747	691	0.0424	648	0.89
FURM 4-1	23.8	0.715	201	5.57	0.946	181.4	0.297	172.5	1.47
FURM 4-2	23.8	0.715	201	3.42	0.593	168.9	0.287	162.4	1.20
FURM 4-3	23.8	0.715	201	2.35	0.437	166.4	0.306	161.7	1.14
FURM 5-1	18.6	0.715	151	2.02	0.372	564	0.0655	546	0.85
FURM 5-2	18.6	0.715	151	4.41	0.747	635	0.0529	599	0.98
FURM 5-3	18.6	0.715	151	5.80	0.989	626	0.0503	583	1.02
FURM 6-1	9.5	0.715	124	3.72	0.631	1504	0.0208	1424	0.88
FURM 6-2	9.5	0.715	124	5.64	0.965	1529	0.0171	1412	0.89
FURM 6-3	9.5	0.715	124	7.88	1.368	1587	0.0151	1435	0.94
FURM 7-1	3.9	0.507	125	3.19	0.512	1251	0.0235	1191	0.80
FURM 7-2	3.9	0.507	125	4.61	0.834	1302	0.0146	1197	0.67
FURM 7-3	3.9	0.507	125	6.83	1.572	1352	0.0141	1221	0.75
FURM 8-1	3.9	0.507	198	1.87	0.362	175.0	0.252	170.4	0.96
FURM 8-2	3.9	0.507	198	4.06	0.646	174.8	0.241	166.8	1.12
FURM 8-3	3.9	0.507	198	6.47	1.202	172.2	0.273	162.6	1.37
FURM 9-1	3.9	0.507	222	1.98	0.390	104.7	0.517	102.2	1.14
FURM 9-2	3.9	0.507	222	3.57	0.567	108.2	0.588	104.7	1.49
FURM 9-3	3.9	0.507	222	7.22	1.361	106.1	0.875	101.8	2.38

*Intracrystalline diffusion model
**Surface barrier model

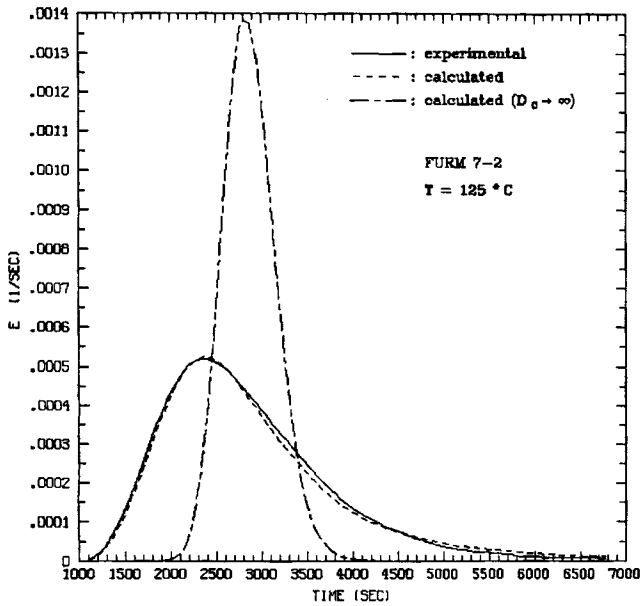

Figure 4. Comparison of calculated and experimental *E* curves for run FURM 7-2, intracrystalline diffusion model.

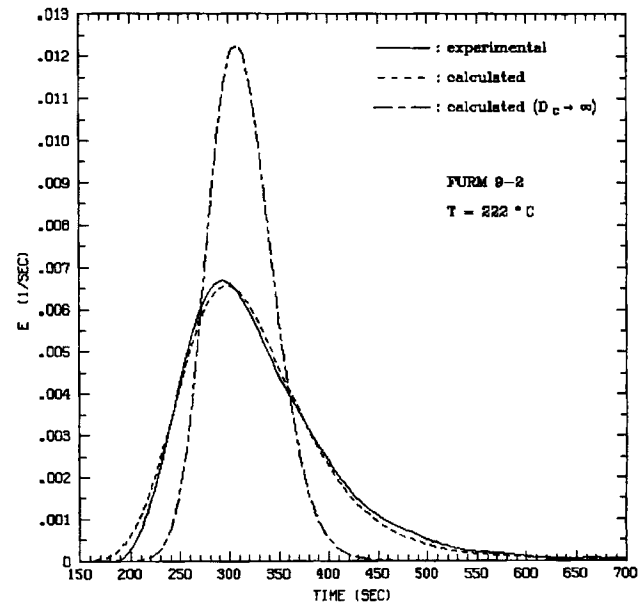

Figure 5. Comparison of calculated and experimental *E* curves for run FURM 9-2, intracrystalline diffusion model.

case is K_c, and $\mathcal{D}_z$ is obtained from the correlation. This curve gives a graphic illustration of the extent to which axial dispersion alone can account for peak broadening. In both cases it is clear that the axial dispersion model is inadequate, and a particle-associated resistance (or resistances) must be affecting the results. It has been demonstrated that axial dispersion at low Reynolds numbers may contain a contribution from intraparticle mass transfer (Wakao and Funazkri, 1978). However, it appears unlikely that this factor can explain our results. Barring a major surface diffusion effect, the overall particle effective diffusivity in the *n*-butane experiments should be lower than same in the methane and ethane experiments that formed the basis of the axial dispersion correlation. The axial dispersion contribution to peak broadening is clearly a larger percentage of the total at the higher temperature, Figure 5. At higher temperatures the particle-associated transport should be more rapid, and ultimately a temperature should be reached where axial dispersion is the only significant contributor to peak broadening.

Small particle sizes were employed in these experiments in order to eliminate a possible contribution from macropore diffusion. Two particle sizes were investigated as an experimental test for this effect. The variation in particle size is not great, but if macropore diffusion is responsible for the particle-associated peak broadening, this contribution should vary as the square of the particle radius ratio, or roughly by a factor of two. No such trend is evident in Table 2 (compare runs FURM 6 and 7 and FURM 1 and 8).

An estimate of the macropore effective diffusivity can be obtained using methods described, for example, in Satterfield (1970). Also, correlations developed for packed beds can be used to obtain an order of magnitude estimate of the convective mass transfer coefficient. We used the correlation of Wakao and Funazkri (1978) for this purpose. Using these estimates, individual contributions of the various terms to peak broadening were calculated from the moments equations (Haynes and Sarma, 1973; Hashimoto and Smith, 1973). The estimated variance contributions for each mass transport effect—axial dispersion, σ_z^2, convective mass transfer, σ_f^2, macropore diffusion, σ_y^2, and intracrystalline diffusion, σ_c^2—expressed as a percentage of the total variance are compiled in Table 3. The major contributors to peak broadening are intracrystalline diffusion and axial dispersion, and the remaining factors are negligible by comparison. It is also evident from this table that the intracrystalline diffusion contribution is reduced at the higher temperatures and lower velocities, making values of diffusivity obtained under such conditions more subject to uncertainty.

A Van't Hoff plot of the Henry's law constants is provided in Figure 6. The data are well correlated by a straight line, and from a least-squares regression one obtains:

$$K_c = 3.06 \times 10^{-3} \exp(5{,}181/T) \qquad (22)$$

The corresponding heat of sorption is $-\Delta H_s = 10.3$ kcal/gmol. The temperature dependence of the intracrystalline diffusivity is well described by the Arrhenius relation, as shown in Figure 7. The equation of the regression line is:

$$\mathcal{D}_c = 1.284 \times 10^{-3} \exp(-7{,}219/T) \qquad (23)$$

with $\mathcal{D}_c$ in cm^2/s. The corresponding diffusional activation energy is $E_d = 14.3$ kcal/gmol.

Table 3. Contributions of Various Mass Transfer Processes to Observed Variance

Run No.	T °C	v cm/s	σ_z^2 %	σ_f^2 %	σ_y^2 %	σ_c^2 %
FURM 1-1	198	4.54	54.43	0.90	1.94	42.73
FURM 1-2	198	4.74	53.00	0.91	1.98	44.12
FURM 1-3	198	2.17	74.87	0.56	1.13	23.44
FURM 2-1	240	2.65	77.12	0.61	1.26	21.01
FURM 2-2	240	4.60	66.26	0.95	2.09	30.70
FURM 2-3	240	6.80	57.37	1.17	2.71	38.75
FURM 3-1	147	4.40	40.63	0.78	1.67	56.92
FURM 3-2	147	4.40	38.48	0.74	1.58	59.20
FURM 3-3	147	4.40	41.33	0.80	1.69	56.17
FURM 4-1	201	5.57	53.49	1.05	2.33	43.13
FURM 4-2	201	3.42	62.76	0.78	1.63	34.83
FURM 4-3	201	2.35	71.73	0.59	1.19	26.50
FURM 5-1	151	2.02	67.81	0.58	1.14	30.47
FURM 5-2	151	4.41	44.63	0.85	1.81	52.71
FURM 5-3	151	5.80	36.53	0.88	1.94	60.64
FURM 6-1	124	3.72	46.88	0.85	1.76	50.51
FURM 6-2	124	5.64	32.97	0.85	1.87	64.31
FURM 6-3	124	7.88	24.76	0.83	1.93	72.47
FURM 7-1	125	3.19	50.07	0.40	0.76	48.78
FURM 7-2	125	4.61	29.56	0.34	0.67	69.44
FURM 7-3	125	6.83	21.20	0.34	0.71	77.74
FURM 8-1	198	1.87	77.60	0.22	0.42	21.75
FURM 8-2	198	4.06	53.84	0.40	0.81	44.95
FURM 8-3	198	6.47	42.23	0.50	1.05	56.22
FURM 9-1	222	1.98	80.56	0.22	0.43	18.79
FURM 9-2	222	3.57	66.60	0.39	0.79	32.22
FURM 9-3	222	7.22	55.62	0.67	1.44	42.27

Analysis based on surface barrier model

The data were subjected to a similar analysis using the surface barrier model. Intracrystalline diffusion was assumed to be infinitely rapid and the adjustable parameters were K_c and k_a. This model also provided an acceptable fit to the data. A typical result is plotted in Figure 8. The optimum model parameters are tabulated in Table 2. As previously observed with the intracrystalline diffusion model, the results are somewhat scattered, but

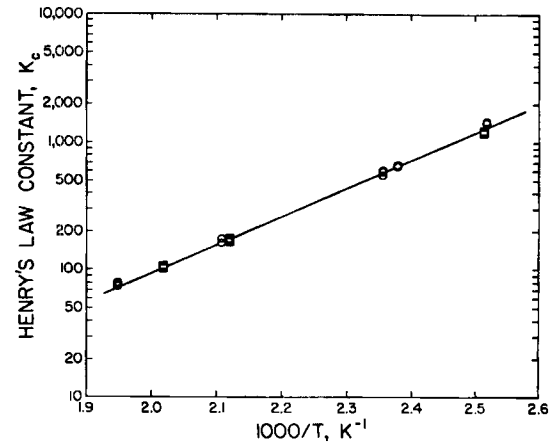

Figure 6. Van't Hoff plot of sorption equilibrium constants.

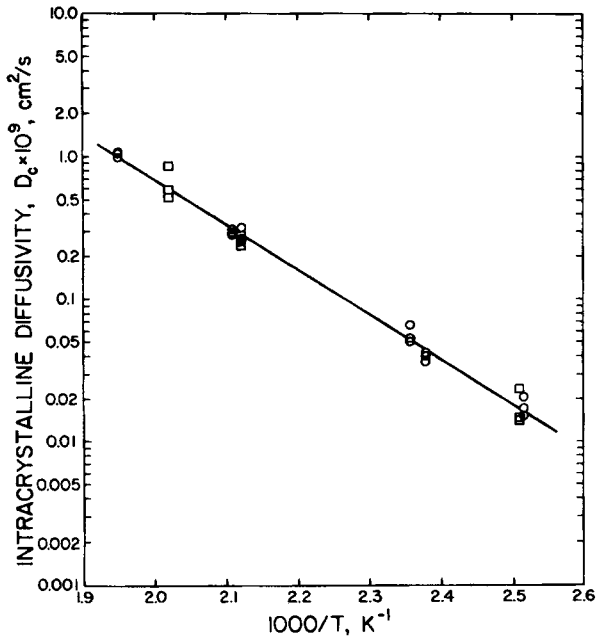

Figure 7. Arrhenius plot of apparent intracrystalline diffusion coefficients.

no clear dependence upon velocity or particle size is evident in the model parameters.

A comparison of Henry's laws constants obtained from the two models indicates that the choice of model has little effect on this parameter. The Van't Hoff plot of Henry's law constants obtained from the surface barrier model is linear and barely distinguishable from the plot of Figure 6. The temperature dependence is given by:

$$K_c = 3.51 \times 10^{-3} \exp(5{,}096/T) \qquad (24)$$

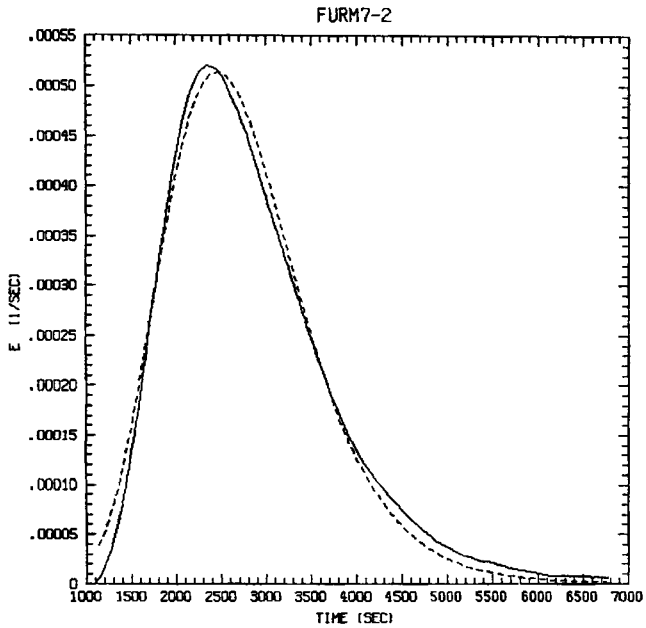

Figure 8. Comparison of calculated and experimental *E* curves for run FURM 7-2, surface barrier model.

and the corresponding heat of sorption is $-\Delta H_s = 10.2$ kcal/gmol. An Arrhenius plot of the sorption rate constants, Figure 9, provides:

$$k_a = 2.37 \times 10^{-2} \exp(-1{,}364/T) \qquad (25)$$

with k_a in cm/s. The activation energy is 2.7 kcal/gmol. Note that while the data in Figure 9 may appear more scattered as compared to the data of Figure 7, this is largely due to the multicyclic logarithmic scale of Figure 7.

Discussion

It is clearly not possible to distinguish between the two models—intracrystalline diffusion resistance and surface barrier—on the basis of their ability to fit the data. Both are entirely consistent with experimental results for the *n*-butane/NaY system. However, the results derived from the intracrystalline diffusion model are in several respects contrary to published reports in the literature. Kärger et al. (1980) have made an extensive study of *n*-paraffins diffusion in NaX zeolites by the NMR technique, and their *n*-butane self-diffusivities are some several orders of magnitude larger than the apparent intracrystalline diffusivities observed in the present study (after extrapolation to a common temperature). In addition, our diffusional activation energy of 14.3 kcal/gmol is far greater than the value of 1.7 kcal/gmol reported by Karger et al. Indeed our value is much higher than the activation energy of 4–5 kcal/gmol Yucel and Ruthven (1980a) found for diffusion of *n*-butane in zeolite 5A, a small-pore zeolite. It does not seem possible to reconcile our values of diffusivity or activation energy with previous literature. Evidently the intracrystalline diffusion limiting model is inapplicable to our system.

On the other hand, the calculated surface barrier parameters appear to be much more in tune with physical reality. The activation energy of 2.7 kcal/gmol is quite reasonable for a physical transport process. Note, however, that had we interpreted our

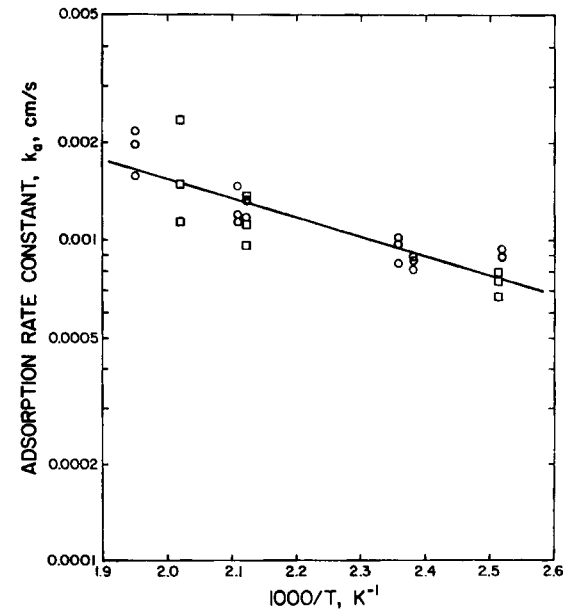

Figure 9. Arrhenius plot of apparent sorption rate constant.

results in terms of k_s, the corresponding activation energy would have been much larger. From Eq. 19 we can write:

$$E_s = E_a - \Delta H_s \tag{26}$$

and therefore $E_s = 2.7 - (-10.1) = 12.8$ kcal/gmol. This value of activation energy implies that the pores at the external surface of the zeolite crystal are severely constricted. There appears to be no *a priori* reason to expect such a strong resistance from surface defects, and we therefore prefer to think of the surface barrier in terms of a finite adsorption rate.

One can call on the kinetic theory of gases (Present, 1958) to calculate the rate at which molecules collide with the external zeolite surface, and from this calculation one can estimate an adsorption rate constant. At 500 K for example, the theoretical value of k_a is 1.07×10^4 cm/s. This does not compare very well at all with the experimental value of $k_a = 1.55 \times 10^{-3}$ cm/s calculated from Eq. 25. The theoretical estimate assumes that all molecules colliding with the external surface enter the crystal interior. The fraction of molecules colliding with the surface which actually enter the zeolite pores (i.e., the sticking coefficient) is evidently of the order of only 1.45×10^{-7}.

Sticking coefficients for physical adsorption on plane surfaces usually lie between 0.1 and 1, and it can be argued effectively that physical adsorption rates are too fast to be observed by pulse gas chromatography (Gangwal et al., 1979). However, when viewed on a microscopic scale the two phenomena—physical adsorption on a plane surface and sorption into a zeolite crystal—are quite different. As discussed, for example, in Laidler (1965) and in Hayward and Trapnell (1964), physically adsorbed molecules are loosely bound to the surface, where they are free to translate in two dimensions. Much of the rotational motion may also be preserved. Absolute rate theory calculations on such a mobile transition state are consistent with the observed sticking factors for physical adsorption.

In contrast, the molecule as it enters the zeolite pore from the gas phase must form a relatively immobile transition complex. All rotational and translational motions are either lost or severely restricted. One can easily calculate sticking coefficients from absolute rate theory of the order of the observed values depending upon the extent to which the transition complex is localized.

As indicated in Table 2, Henry's law constants calculated from the diffusion limiting model and the surface barrier model are practically the same. This is expected since K_c is related to the first moment of the chromatogram (i.e., retention time), and the first moment is independent of the mass transport parameters (Haynes and Sarma, 1973). Several studies of *n*-butane sorption on zeolite NaX have been reported. Most authors report an isosteric heat of sorption, $\Delta H'_s$, which can be calculated from the isochor heat, ΔH_s, according to the relation (Barrer and Barrie, 1952):

$$-\Delta H'_s = -\Delta H_s + RT \tag{27}$$

At 500 K this equation gives an isosteric heat of sorption of $-\Delta H'_s = 11.1$ kcal/gmol for our data. This value compares favorably with values of $-\Delta H'_s = 14.2$ kcal/gmol and $-\Delta H'_s = 9.3$ kcal/gmol reported by Barrer and Sutherland (1956) and by Doelle and Riekert (1979), respectively.

It is important to realize that our study employed very small crystals of a large-pore zeolite, and it is therefore not unreasonable that the surface barrier resistance should dominate. In other studies of diffusion in large crystals and/or small-pore zeolites in the intracrystalline diffusion resistance dominates. Sorption rate studies for N_2, CH_4, and C_2H_6 (Yucel and Ruthven, 1980b) and CO_2 (Yucel and Ruthven, 1980c) in zeolite 4A yielded diffusivities independent of crystallite size. Similarly, the uptake of CF_4 and n-C_4H_{10} in large crystals of zeolite 5A was dominated by intracrystalline diffusion (Yucel and Ruthven, 1980a). A general analysis must account for both effects, but as observed in our study, it may not be possible to separate these effects on the basis of goodness of fit. Pulse chromatography experiments on samples prepared from different crystallite size zeolites should prove informative in this regard.

Acknowledgment

Several individuals have assisted us in the crystallite size analysis. M. P. Mathur of the U.S. Department of Energy, P.E.T.C. performed the microscopic analysis. M.L. Occelli of the Gulf Research and Development Co. analyzed the sample by SEM and also performed conductometric analyses. The sedimentation analysis was carried out under the direction of W.H. Flank of the Linde Division of Union Carbide. In addition to providing the measurements, all these individuals have contributed to our understanding of size distribution analysis.

Notation

C_y = gas phase concentration of diffusing species, gmol/mL
D = quantities, Eqs. 2, 3
$\mathcal{D}_c$ = intracrystalline diffusion coefficient, cm^2/s
$\mathcal{D}_y$ = macropore diffusion coefficient
$\mathcal{D}_z$ = axial dispersion coefficient, cm^2/s
E = transformed residence time distribution curve
E_a = activation energy for adsorption rate constant, kcal/gmol
E_d = activation energy for intracrystalline diffusion, kcal/gmol
E_s = activation energy for surface barrier coefficient, kcal/gmol
F = quantities, Eqs. 5, 6
G = quantities, Eqs. 7, 8
H = quantities, Eqs. 11, 12
ΔH_s = isochor heat of sorption, kcal/gmol
$\Delta H'_s$ = isosteric heat of sorption, kcal/gmol
I = quantities, Eqs. 9, 10 (intracrystalline diffusion model) or Eqs. 15, 16 (surface barrier model)
k_a = adsorption rate constant, cm/s
k_s = surface barrier coefficient, cm/s
K_c = Henry's law constant
L = column length, cm
p = variable of integration
Pe = particle Peclet number
q = sorbed phase concentration
R = gas constant, kcal/gmol · K
R_x = crystallite radius, cm
Re = particle Reynolds number
Sc = fluid Schmidt number
T = temperature, K
v = superficial velocity, cm/s

Greek letters

θ = angle, Eq. 4
θ_y = macropore porosity, mL macropore/mL particle
θ_z = bed porosity, mL bed void/mL bed
λ = quantity, Eq. 13
μ = parameter in log-normal crystal size distribution
σ = parameter in log-normal crystal size distribution
σ^2 = variance of residence time distribution

Literature cited

Barrer, R. M., and J. A. Barrier, "Sorption and Surface Diffusion in Porous Glass," *Proc. Ray. Soc. A*, **213**, 250 (1952).
Barrer, R. M., and J. W. Sutherland, "Inclusion Complexes of Faujasite

with Paraffins and Permanent Gases," *Proc. Ray. Soc. A* **237,** 439 (1956).
Bülow, M., P. Struve, G. Finger, C. Redszus, K. Ehrhardt, W. Schirmer, and J. Kärger, "Sorption Kinetics of *n*-Hexane on MgA Zeolites of Different Crystal Sizes. Study of the Rate-Limiting Transport Mechanism," *J. Chem. Soc., Faraday Trans. I,* **76,** 597 (1980).
Bülow, M., P. Struve, W. Mietk, and M. Kocirik, "Experimental Evidence of the Influence of Sorption-Heat Release Processes on the Sorption Kinetics of Benzene in NaX Zeolite Crystals," *J. Chem. Soc., Faraday Trans. I,* **80,** 813 (1984).
Cerro, R. L., and J. M. Smith, "Effects of Heat Release and Nonlinear Equilibrium on Transient Adsorption," *Ind. Eng. Chem. Fund.,* **8,** 796 (1969).
Chou, T. S., "Design of a Pulse Diffusivity Apparatus for Improved Sensitivity," *Chem. Eng. Sci.,* **34,** 133 (1979).
Doelle, H. J., and L. Riekert, "Kinetics of Sorption, Desorption and Diffusion in Zeolites," *Angew. Chem., Int. Ed. Engl.,* **18,** 266 (1979).
Fu, C. C., "Diffusion of *n*-Butane in Zeolite NaY," M.S. Thesis, Univ. Wyoming, Laramie (Dec., 1984).
Gangwal, S. K., R. R. Hudgins, and P. L. Silveston, "Reliability and Limitations of Pulse Chromatography in Evaluating Properties of Flow Systems. 1: Modeling and Experimental Considerations," *Can. J. Chem. Eng.,* **57,** 609 (1979).
Hashimoto, N., and J. M. Smith, "Macropore Diffusion in Molecular Sieve Pellets by Chromatography," *Ind. Eng. Chem. Fund.,* **12,** 335 (1973).
Haynes, H. W., Jr., "The Determination of Effective Diffusivity by Gas Chromatography. Time Domain Solutions," *Chem. Eng. Sci.,* **30,** 955 (1975).
———, "An Analysis of Sorption Heat Effects in the Pulse Gas Chromatography Diffusion Experiment," to be published in the *AIChE J.,*1986.
Haynes, H. W., Jr. and P. N. Sarma, "A Model for the Application of Gas Chromatography to Measurements of Diffusion in Bidisperse Structured Catalysts," *AIChE J.,* **19,** 1043 (1973).
Hayward, D. O., and B. M. W. Trapnell, *Chemisorption,* Butterworths, Washington, DC (1964).
Hsiang, T. C. S., and H. W. Haynes, Jr., "Axial Dispersion in Small-Diameter Beds of Large, Spherical Particles," *Chem. Eng. Sci.,* **32,** 678 (1977).
Hsu, L. K. P., and H. W. Haynes, Jr., "Effective Diffusivity by the Gas Chromatography Technique: Analysis and Application to Measurements of Diffusion of Various Hydrocarbons in Zeolite NaY," *AIChE J.,* **27,** 81 (1981).
Kärger, J., and J. Caro, "Interpretation and Correlation of Zeolite Diffusivities Obtained from Nuclear Magnetic Resonance and Sorption Experiments," *J. Chem. Soc., Faraday Trans. I,* **73,** 1363 (1977).
Kärger, J., and D. M. Ruthven, "Diffusion in Zeolites," *J. Chem. Soc., Faraday Trans. I,* **77,** 1485 (1981).
Kärger, J., H. Pfeifer, M. Rauscher, and A. Walter, "Self-diffusion of *n*-Paraffins in NaX Zeolite," *J. Chem. Soc., Faraday Trans. I,* **76,** 717 (1980).
Koresh, J., and A. Soffer, "Molecular Sieve Carbons. 3: Adsorption Kinetics According to a Surface-barrier Model," *J. Chem. Soc., Faraday Trans. I,* **77,** 3005 (1981).
Laidler, K. J., *Chemical Kinetics,* McGraw-Hill, New York (1965).
Lee, L. K., and D. M. Ruthven, "Analysis of Thermal Effects in Adsorption Rate Measurements," *J. Chem. Soc., Faraday Trans. I,* **75,** 2406 (1979).
Present, R. D., *Kinetic Theory of Gases,* McGraw-Hill, New York (1958).
Ruthven, D. M., Diffusion in A, X, and Y Zeolites," *ACS Symp. Ser.,* **218,** 345 (1983).
———, *Principles of Adsorption and Adsorption Processes,* Wiley, New York (1984).
Ruthven, D. M., and L. K. Lee, "Kinetics of Nonisothermal Sorption: Systems with Bed Diffusion Control," *AIChE J.,* **27,** 654 (1981).
Ruthven, D. M., L. K. Lee, and H. Yucel, "Kinetics of Nonisothermal Sorption in Molecular Sieve Crystals," *AIChE J.,* **26,** 16 (1980).
Satterfield, C. N., *Mass Transfer in Heterogeneous Catalysis,* M.I.T. Press, Cambridge, MA (1970).
Shah, D. B., and D. M. Ruthven, "Measurements of Zeolitic Diffusivities and Equilibrium Isotherms by Chromatography," *AIChE J.,* **23,** 804 (1977).
Wakao, N., and T. Funazkri, "Effect of Fluid Dispersion Coefficients on Particle-To-Fluid Mass Transfer Coefficient in Packed Beds—Correlation of Sherwood Numbers," *Chem. Eng. Sci.,* **33,** 1375 (1978).
Yucel, H., and D. M. Ruthven, "Diffusion in 5A Zeolite. Study of the Effect of Crystal Size," *J. Chem. Soc., Faraday Trans. I,* **76,** 71 (1980a).
———, "Diffusion in 4A Zeolite. Study of the Effect of Crystal Size," *J. Chem. Soc., Faraday Trans. I,* **76,** 60 (1980b).
———, "Diffusion of CO_2 in 4A and 5A Zeolite Crystals," *J. Coll. Interf. Sci.,* **74,** 186 (1908c).

Manuscript received May 15, 1985, and revision received Mar. 14, 1986.